

3D Densification for Multi-Map Monocular VSLAM in Endoscopy

X. Anadón, Javier Rodríguez-Puigvert, J.M.M. Montiel

Universidad de Zaragoza, Zaragoza, Spain
{xanadon,jrp,josemari}@unizar.es
Preprint

Abstract. Multi-map Sparse Monocular visual Simultaneous Localization and Mapping applied to monocular endoscopic sequences has proven efficient to robustly recover tracking after the frequent losses in endoscopy due to motion blur, temporal occlusion, tools interaction or water jets. The sparse multi-maps are adequate for robust camera localization, however they are very poor for environment representation, they are noisy, with a high percentage of inaccurately reconstructed 3D points, including significant outliers, and more importantly with an unacceptable low density for clinical applications.

We propose a method to remove outliers and densify the maps of the state of the art for sparse endoscopy multi-map CudaSIFT-SLAM. The NN LightDepth for up-to-scale depth dense predictions are aligned with the sparse CudaSIFT submaps by means of the robust to spurious LMedS. Our system mitigates the inherent scale ambiguity in monocular depth estimation while filtering outliers, leading to reliable densified 3D maps. We provide experimental evidence of accurate densified maps 4.15 mm RMS accuracy at affordable computing time in the C3VD phantom colon dataset. We report qualitative results on the real colonoscopy from the Endomapper dataset.

1 Introduction

Dense 3D reconstruction of endoscopic images is critical for enhancing visualization in medical procedures, assisting clinicians during interventions, and enabling autonomous robotic systems. 3D dense representation of the organ could help physicians assess lesion sizes, ensure complete mucosa coverage, and minimize the risk of missing critical areas during exploration [18]. However, the endoscopy environment is challenging characterized by low-texture regions, dynamic lighting and abrupt camera movements, making it particularly challenging to obtain reliable 3D dense reconstructions.

Multi-maps feature-based Monocular visual Simultaneous Localization and Mapping achieve accurate camera tracking, producing sparse 3D reconstructions that are too noisy and lacking in detail for clinical use. CudaSIFT-SLAM[7] have demonstrated real-time performance and robust camera tracking, nevertheless their sparse representation limits its applicability. To overcome these limitations, we propose a 3D dense multi-mapping system that combines the robust

camera tracking of a feature-based SLAM with the dense depth prediction of a single-view self-supervised depth estimation. Our system integrates the sparse maps from CudaSIFT-SLAM with the up-to-scale predictions of LightDepth[24] aligning them using Least Median Squares(LMedS)[28] for scale corrections and outlier filtering. Our method achieves a densification of the multi-maps while maintaining the camera pose accuracy during the endoscope trajectory.

We propose a robust method that aligns dense up-to-scale predictions with sparse points to achieve dense reconstructions. It has the following contributions:

- Dense 3D surface reconstruction in less than 200 ms, which makes it suitable for real-time applications.
- Experimental validation on the C3VD dataset, including full screening sequences, and qualitative tests on real colonoscopy recordings from the Endomapper dataset.
- Removing the need for domain adaptation, as the components of the system are agnostic to domain specifications.

2 Related Work

Feature-based SLAM [20] has been successfully applied to abdominal endoscopy in [17] computing reliable 3D poses for the video frames as a first step towards a multiview stereo densification based on correlation matching between pixel frames. It is assumed a rigid scene. Focused in endoscopic endonasal surgery, SAGE SLAM [13] proposes to use a depth network[27] that corrects a global scale in a deep feature SLAM pipeline. Discrete features has been also exploited to handle deforming tissue, NR-SLAM [26] combines a Dynamic Deformation Graph with a Visco-Elastic deformation model, allowing automatic initialization and extension of a sparse point cloud in deforming environments.

However, feature-based systems struggled with low-texture regions and feature scarcity, limiting their robustness for real procedures, specially in colonoscopy. In any case, CudaSIFT-SLAM [7], based on ORB-SLAM3 [4] leveraging CudaSIFT features, has demonstrated real-time performance and high accuracy in recovering the camera pose by incorporating a quasi-rigid deformation model for monocular colonoscopy sequences. CudaSIFT-SLAM[7] ability to merge multiple maps and perform relocalization enables tracking recovery, making it particularly effective for exploratory trajectories in endoscopy, where unpredictable motion and occlusions often cause tracking failures. In clinical settings, feature-based SLAM is restricted due to the sparse representation where a dense representation is essential.

Direct methods have also been explored to achieve 3D dense reconstruction in endoscopy, mainly based on the minimization of a photometric residual for camera tracking in combination with a depth estimation network for densification. Endo-Depth[23] uses [9] with photometric residual-based camera tracking. RNN-SLAM [16] integrates DSO [8] with a recurrent neural network, leveraging temporal dependencies to refine depth and pose estimation [32]. Direct methods, however, lack of loop closing detection, multi-mapping, and are unable to

recover from camera tracking losses, what limits their performance in realistic colonoscopy scenes where tracking losses and map fragmentation is prevalent.

Depth perception plays an crucial role when it comes to 3D dense reconstructions from endoscopic images. Supervised methods rely on annotated datasets[30], and the lack of depth-annotated endoscopic data limits their use. Multi-view self-supervision has been addressed for endoscopic images [15,11], but remains challenging due to the presence of deformations, weak texture and specular reflections. Synthetic-to-real domain adaptation has been addressed with GAN models[22,12,33] and with teacher-student architectures[25,21]. Single-View self-supervised learning has emerged [24] exploiting the illumination decline as a natural depth cue in the endoscopic setting where the camera and light are co-located. In contrast to multi-view methods and supervised approaches, LightDepth can be trained directly from individual frames, providing a scalable solution without the need for explicit ground truth depth annotations.

3D Dense Reconstructions based on NeRFs and 3D Gaussian splatting have been also explored for endoscopic images, although with primarily focus on rendering quality, rather than explicitly modeling the geometric accuracy of the reconstructed scene. Wang et al.[34] proposes the use of NeRFs for known cameras and stereo depth in deformable laparoscopic scenes. FreeSurgGS[10] proposes a combination of SfM and 3D Gaussian splatting for optimization of the camera poses and scene representation. EndoGSLAM[31] propose a dense RGB-D SLAM approach based on the 3D Gaussian representation and differentiable rasterization for tracking and tissue reconstruction. However, these methods rely on stereo or depth sensors, which are not available in standard monocular endoscopes. In contrast, we propose a monocular-based approach tailored for conventional endoscopic imaging without additional depth sensing hardware. Beltran et al. [6] introduced bundle adjustment improvements using supervised depth from [21] into EndoGSLAM pipeline. Building upon RNN-SLAM[16], Gaussian Pancakes [3] improves the 3D Gaussian Splatting representation with geometric generalization. Focusing on the quality of 3D reconstruction, LightNeus [2] models surfaces with known camera poses. Exploiting the illumination decline principle, it employs a neural implicit representation to compute the 3D surface reconstruction.

3 System Overview

Our system builds a 3D dense multi-map representation of the environment and simultaneously localizes the camera pose with respect to the multi-maps. We built on two systems able to operate in real colonoscopy environments, CudaSIFT-SLAM[7], a feature-based monocular SLAM and LightDepth, [24] a self-supervised single-view depth prediction network based on illumination decline.

CudaSIFT-SLAM multiple-map approach is able to perform with numerous merges that avoid over-segmentation of the sub-maps. Each of those submaps, \mathcal{M} , is defined as a sparse set of 3D points, represented in world reference coordi-

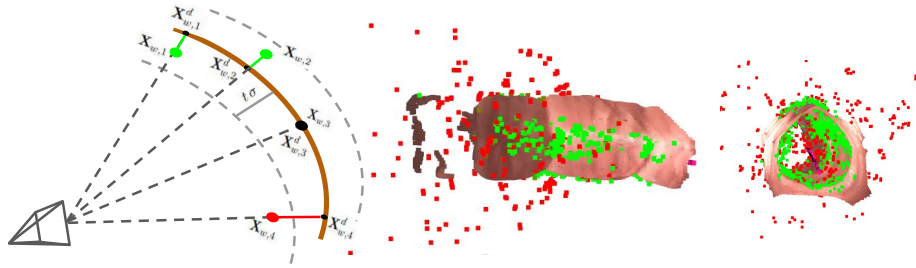


Fig. 1: 3D dense submap. Left, 2D simplified plot of the LMedS inlier-outlier boundary. Middle and right, two views of the dense model along with the sparse map points. Green: LMedS inlier sparse map points after. Red: outliers.

nates as $\{\mathbf{X}_{w,j}\} \subset \mathbb{R}^3$, and a set of selected frames, $\{K_i\}$, called keyframes, whose localization is defined as a transformation in the world reference $\{\mathbf{T}_{iw}\} \subset \text{SE}(3)$. Each \mathcal{M} has its own scale, as scale is typically not observable in monocular SLAM. These maps can be understood as a summary of visual and geometric information of what was seen during the procedure. Although the submaps $\{\mathbf{X}_{w,j}\}$ yield by CudaSIFT-SLAM are useful for camera pose estimation, they are inherently sparse and noisy.

For each keyframe K_i in a CudaSIFT submap \mathcal{M} , LightDepth predicts a depth map $d_i \in (0, \infty)^{w \times h}$ and an albedo map $\rho_i \in [0, 1]^{w \times h \times 2}$.

In the photometric model of LightDepth, the gain is fixed at 1 for all input images, allowing the network to adjust depth estimates d_i to account for variations in brightness, particularly in darker regions resulting up-to-scale depth estimation with a different scale per each keyframe. To achieve clinically meaningful dense reconstructions, we combine the up-to-scale LightDepth depth maps d_i with the sparse submap points $\{\mathbf{X}_{w,j}\}$.

Per each keyframe K_i , we compute the scale s_i that aligns its depth map d_i with the 3D sparse point cloud $\{\mathbf{X}_{w,j}\}$ minimizing the distance between the sparse map points and the dense depth. The sparse map points are very noisy, and a high fraction of them are spurious. We opt for LMedS because it can compute from scratch the distance threshold to determine if a map point is spurious. Pre-defining a fixed distance threshold is not possible because of the unknown scale for the sparse map, and because of the strong dependence of the 3D point error with the point depth due to the non-linearities of the triangulation, hence RANSAC cannot be applied.

Per each map point $\mathbf{X}_{w,j}$ we compute a scale proposal:

$$s_{i,j} = \frac{\|\mathbf{X}_{w,j}\|}{\|\mathbf{X}_{w,j}^d\|}, \quad \mathbf{X}_{w,j}^d = \pi_i^{-1}(\pi_i(\mathbf{T}_{iw}, \mathbf{X}_{w,j}), \mathbf{T}_{iw}, d_i) \quad (1)$$

Where $\pi_i(\cdot)$ defines the projection of a map point in camera i and $\pi_i^{-1}(\cdot)$ yields, $\mathbf{X}_{w,j}^d$ the unprojection in 3D of an image pixel, assigning the depth according to the depth map d_i .

Each scale proposal is ranked according to the median of the squared residuals for all sparse points in the map, selecting as the scale the one producing the smallest median residual:

$$s_i^{\text{LMedS}} = \arg \min_{s_{i,j}} \text{median}(\{\epsilon_{i,j,k}^2\}) \quad k \neq j, \quad \epsilon_{i,j,k} = \|\mathbf{X}_{w,k} - s_{i,j} \mathbf{X}_{w,k}^d\| \quad (2)$$

This first estimate of the scale allows to define error standard deviation for the inliers as $\sigma = 1.4826\sqrt{\min_m}$, being \min_m the minimal median squared residual yield by $s_{i,j}^{\text{LMedS}}$. The $t\sigma$ defines a threshold to identify the inlier map points:

$$\|\mathbf{X}_{w,k} - s_{i,j}^{\text{LMedS}} \mathbf{X}_{w,k}^d\| \geq t\sigma \quad (3)$$

The inlier map points are used to refine the scale by means of a non-linear optimization:

$$s_i = \arg \min_{s_i} \sum_k r_k \left(\|\mathbf{X}_{w,k} - s_i \mathbf{X}_{w,k}^d\|^2 \right) \quad k \text{ inlier} \quad (4)$$

being r_k a robust influence function and using s_i^{LMedS} as initial guess.

We have a scaled RGBD observation per each keyframe. As we also have the pose of the keyframe, we use *Truncated Signed Distance Function (TSDF)* [5], in its Open3D implementation [35], to fuse all the scaled RGBD observations in a unique surface. Then the global surface can be explicitly extracted using the *Marching Cubes* algorithm [14].

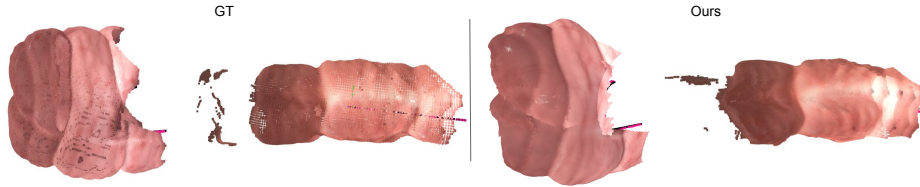


Fig. 2: Dense 3D reconstruction for Transverse t2a and Cecum c2a.

4 Experimental Results

Quantitative results in C3VD. C3VD balances realism with the availability of accurate ground truth labels. It captures the imaging conditions of a real endoscope, including illumination inverse squared decay, global illumination effects and specular highlights. The dataset includes short sequences and screening sequences. The short sequences contain ground-truth in pose, depth and surface normals derived by registering the 2D endoscopic images to corresponding 3D phantom models. The camera trajectory is short, with a slow motion, and the

Metrics	Short Sequences									Screening Sequences				
	t2a	t3a	t4a	c1a	c2a	c3a	d4a	s3a	Avg	Seq1	Seq2	Seq3	Seq4	Avg
# Frames	194	250	382	276	370	730	148	613	370	5458	5100	4726	4774	5015
# KF	16	7	14	21	24	15	11	42	19	467	687	565	381	525
KF time	243	714	546	263	308	973	269	292	451	234	148	167	251	200
RMS ATE	0.58	0.17	0.43	0.47	0.79	0.54	0.17	0.48	0.45	3.39	2.94	2.80	3.25	3.10

Table 1: CudaSIFT-SLAM performance on C3VD. The RMS ATE is in mm and the KF time in ms.

Method	Metrics	t2a	t3a	t4a	c1a	c2a	c3a	d4a	s3a	avg
CudaSift	#MP ($\times 10^3$)	1.8	1.5	2.4	1.8	2.4	2.0	2.4	1.8	2.0
	RMS Acc. ↓	242.73	6.84	44.09	21.54	72.50	58.32	192.69	153.87	99.07
	MedA Acc. ↓	2.11	1.75	1.04	3.7	1.64	3.21	1.05	1.60	2.01
Ours	#MP ($\times 10^3$)	98	34	54	555	148	83	64	34	134
	RMS Acc. ↓	2.46	4.39	3.13	4.55	3.97	6.06	5.23	3.39	4.15
	MedA Acc. ↓	1.68	3.15	1.70	3.13	2.42	2.75	3.70	2.26	2.60
LightNeus[2]	RMS Acc. ↓	2.58	10.70	3.79	2.01	1.87	5.49	4.08	3.18	4.21
	MedA Acc. ↓	2.24	6.39	1.15	0.95	1.40	1.12	2.66	2.57	2.31

Table 2: Dense maps performance. All the Accuracies: RMS Acc. and MedA Acc. are in mm.

camera far from the colon surfaces. The screening sequences contain only ground-truth camera poses. Regarding the camera movement, it is fast because it mimics the withdrawal phase of a screening colonoscopy. In many cases there is motion blur and the camera can be very close to the colon surfaces.

We present the quantitative results on 8 C3VD short test sequences following the train/test split of LightDepth DPT [24] (See Figure 2). We report in Table 1 the performance of CudaSIFT, after alignment with GT by means of the similarity transformation, i.e. rotation, translation and scale that minimizes the ATE between the CudaSIFT estimated camera trajectory and the GT camera trajectory. The camera trajectory achieves a 0.45 mm ATE. On average, the sequences are 370 frames long, are summarized in 19 keyframes what leaves 375 ms to deal with the densification of each keyframe.

We report in Table 2 the density as the map number of map points (#MP) either in CudaSIFT and after the proposed densification. Regarding accuracy, we report RMS Accuracy and the MedA Accuracy. The accuracy [29] is defined as the distance from each point of our 3D model to its closest in the GT in mm. The ground truth point cloud is obtained by unprojecting the ground truth depths from ground truth camera poses. For alignment we use the similarity transformation that aligns the CudaSIFT-SLAM trajectory with the GT trajectory to minimize the ATE. We also include as baseline LightNeus [2] a state-of-the-art 3D reconstruction based on neural rendering exploring the illumination decline principle and coding dense model with a TSDF as we do.

Our densification method increase the number of points by factor bigger than 60. Regarding the accuracy, CudaSIFT-SLAM accuracy is 2.01 mm in MedA but 99 mm in RMS values, showing clearly that the sparse map has a 50% of accurate map points, but there are plenty spurious points that the geometrical methods are not able to remove. When combined with the LightDepth dense depth prediction, both the density and the RMS Accuracy boost. Regarding the comparison with LightNeus we are able to produce maps with comparable accuracy, at a fraction of the computational cost and not needing the GT camera poses. Note that, as baseline, LightDepth reports a per frame RMSE 5.60 mm and MedAE 2.67 mm for single-view depth estimation errors. Thanks to the fusion of accumulative predictions in depth, we achieve a better performance than LightDepth in our after fusion dense maps.

Regarding the computing time, our densification method requires in total 186 ms below the 200 ms available per KF. LightDepth inference last for 22 ms, the LMedS scale alignment 138 ms and the TSDF integration 26 ms. The Marching Cubes algorithm takes 117 ms. All experiments were conducted on an Intel i7 CPU, operating at 3.6GHz, with 32 GB of memory, and utilizing an NVIDIA TITAN V GPU.

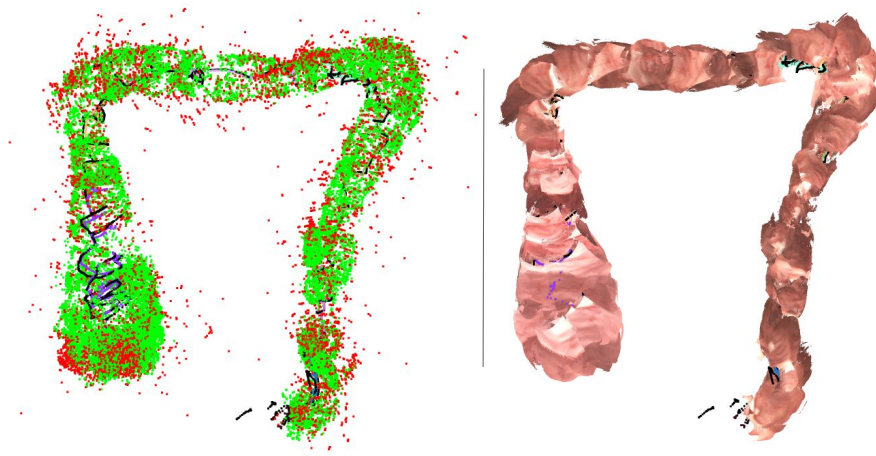


Fig 3: Results for screening Seq3. Left sparse maps, red outliers, green inliers according to LMedS. Right, dense 3D reconstruction

When processing the 4 screening sequences, CudaSIFT-SLAM produces multiple maps (19 maps on average) along the trajectory due to camera occlusions and tracking failure. Regarding the trajectory we reach a 3.09 mm RMS ATE for the camera trajectory while locating in the map 83.32% of the frames in each sequence. Compared to the a 0.45 mm RMS ATE obtained in short sequences (Table 1) we observe a significant increase, showing the greater challenge of the screening explorations. Figure 3 shows our 3D dense map for Seq3. It is also

displayed the capability to detect and reject spurious in the CudaSIFT-SLAM sparse map.

Qualitative results We have conducted qualitative experiments on the En-

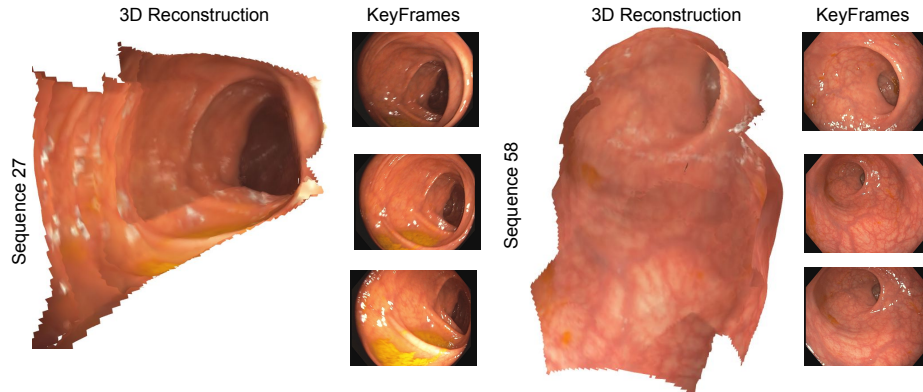


Fig. 4: Dense maps in EndoMapper in Seq_027 and Seq_058

doMapper dataset [1], because it includes real screening procedures with water jets, occlusions, deformation or motion blur. Additionally, it is provided an accurate colonoscope calibration both geometric and photometric. We have trained LightDepth DPT[24] on 42 384 EndoMapper [1] images selected using covisibility according to ColonMapper[19].

We provide qualitative results (Figure 4) in sequences Seq_027 and Seq_038 from the EndoMapper dataset, building 3D models from the sole input of the images coming from a standard monocular colonoscope.

5 Conclusions

The proposed CudaSIFT-SLAM + LightDepth combination has proven able to successfully clean from spurious and densify the sparse multi-maps that enable robust camera tracking in real endoscopies.

Our approach addresses the inherent scale ambiguity in monocular depth estimation NN’s by robustly aligning dense up-to-scale depth predictions to the single scale of the sparse 3D map by means of a Least Median Squares strategy followed by a non-linear optimization. Experimental results on the C3VD and Endomapper datasets demonstrate that our method achieves competitive accuracy against state-of-the-art techniques.

Future work we will explore the integration of the NN depth estimates into the sequential real-time V-SLAM pipeline, including the initialization, relocation and bundle adjustment for the local mapping.

References

1. Azagra, P., et al.: EndoMapper dataset of complete calibrated endoscopy procedures. *Scientific Data* **10**(1), 671 (2023)
2. Batlle, V.M., Montiel, J.M.M., Fua, P., Tardós, J.D.: LightNeuS: Neural surface reconstruction in endoscopy using illumination decline. In: *MICCAI*. pp. 503–513. Springer (2023)
3. Bonilla, S., Zhang, S., Psychogyios, D., Stoyanov, D., Vasconcelos, F., Bano, S.: Gaussian Pancakes: Geometrically-Regularized 3D Gaussian Splatting for Realistic Endoscopic Reconstruction. *arXiv* (2024)
4. Campos, C., Elvira, R., Gomez, J.J., Montiel, J.M.M., Tardós, J.D.: ORB-SLAM3: An accurate open-source library for visual, visual-inertial and multi-map SLAM. *IEEE Transactions on Robotics* **37**(6), 1874–1890 (2021)
5. Curless, B., Levoy, M.: A volumetric method for building complex models from range images. In: *Proceedings of the 23rd annual conference on Computer graphics and interactive techniques*. pp. 303–312 (1996)
6. Dunn Beltran, A., Rho, D., Niethammer, M., Sengupta, R.: Nfl-ba: Improving endoscopic slam with near-field light bundle adjustment. In: *arXiv preprint arXiv:2412.13176* (2024)
7. Elvira, R., Tardós, J.D., Montiel, J.M.M.: CudaSIFT-SLAM: multiple-map visual SLAM for full procedure mapping in real human endoscopy. *arXiv preprint arXiv:2405.16932* (2024)
8. Engel, J., Koltun, V., Cremers, D.: Direct sparse odometry. *IEEE Transactions on Pattern Analysis and Machine Intelligence* **40**(3), 611–625 (2018)
9. Godard, C., Mac Aodha, O., Firman, M., Brostow, G.J.: Digging into self-supervised monocular depth prediction. *ICCV* (October 2019)
10. Guo, J., Wang, J., Kang, D., Dong, W., Wang, W., Liu, Y.h.: Free-surgs: Sfml-free 3d gaussian splatting for surgical scene reconstruction. In: *MICCAI*. Springer (2024)
11. Huang, B., Zheng, J.Q., Nguyen, A., Tuch, D., Vyas, K., Giannarou, S., Elson, D.S.: Self-supervised generative adversarial network for depth estimation in laparoscopic images. In: *MICCAI* (2021)
12. Karaoglu, M.A., Brasch, N., Stollenga, M., Wein, W., Navab, N., Tombari, F., Ladikos, A.: Adversarial domain feature adaptation for bronchoscopic depth estimation. In: *MICCAI*. pp. 300–310. Springer (2021)
13. Liu, X., Li, Z., Ishii, M., Hager, G.D., Taylor, R.H., Unberath, M.: Sage: Slam with appearance and geometry prior for endoscopy. In: *2022 International Conference on Robotics and Automation (ICRA)*. pp. 5587–5593 (2022)
14. Lorensen, W.E., Cline, H.E.: Marching cubes: A high resolution 3d surface construction algorithm. *SIGGRAPH Comput. Graph.* **21**(4), 163–169 (Aug 1987)
15. Luo, H., Hu, Q., Jia, F.: Details preserved unsupervised depth estimation by fusing traditional stereo knowledge from laparoscopic images. *Healthcare Technology Letters* **6**(6), 154 (2019)
16. Ma, R., Wang, R., Zhang, Y., Pizer, S., McGill, S.K., Rosenman, J., Frahm, J.M.: RNNSLAM: Reconstructing the 3D colon to visualize missing regions during a colonoscopy. *Medical image analysis* **72**, 102100 (2021)
17. Mahmoud, N., Collins, T., Hostettler, A., Soler, L., Doignon, C., Montiel, J.M.M.: Live tracking and dense reconstruction for handheld monocular endoscopy. *IEEE transactions on medical imaging* **38**(1), 79–89 (2018)

18. Metzger, R., Suppa, P., Li, Z., Vemuri, A.: Augmented reality navigation systems in endoscopy. *Frontiers in Gastroenterology* **3** (2024)
19. Morlana, J., Tardós, J.D., Montiel, J.: ColonMapper: topological mapping and localization for colonoscopy. In: *IEEE ICRA*. pp. 6329–6336 (2024)
20. Mur-Artal, R., Montiel, J.M.M., Tardós, J.D.: ORB-SLAM: a versatile and accurate monocular SLAM system. *IEEE Trans. on Robotics* **31**(5), 1147–1163 (2015)
21. Paruchuri, A., Ehrenstein, S., Wang, S., Fried, I., Pizer, S.M., Niethammer, M., Sengupta, R.: Leveraging Near-Field Lighting for Monocular Depth Estimation from Endoscopy Videos. In: *ECCV*. Springer (2024)
22. Rau, A., Edwards, P.E., Ahmad, O.F., Riordan, P., Janatka, M., Lovat, L.B., Stoyanov, D.: Implicit domain adaptation with conditional generative adversarial networks for depth prediction in endoscopy. *International Journal of Computer Assisted Radiology and Surgery* pp. 1–10 (2019)
23. Recasens, D., Lamarca, J., Fácil, J.M., Montiel, J.M.M., Civera, J.: Endo-Depth-and-Motion: Reconstruction and Tracking in Endoscopic Videos Using Depth Networks and Photometric Constraints. *IEEE Robotics and Automation Letters* **6**(4), 7225–7232 (2021)
24. Rodríguez-Puigvert, J., Batlle, V.M., Montiel, J., Martínez-Cantin, R., Fua, P., Tardós, J.D., Civera, J.: LightDepth: Single-View Depth Self-Supervision from Illumination Decline. In: *ICCV*. pp. 21273–21283 (October 2023)
25. Rodríguez-Puigvert, J., Recasens, D., Civera, J., Martínez-Cantin, R.: On the Uncertain Single-View Depths in Colonoscopies. In: *MICCAI*. pp. 130–140. Springer (2022)
26. Rodríguez, J.J.G., Montiel, J.M., Tardós, J.D.: NR-SLAM: Nonrigid monocular SLAM. *IEEE Transactions on Robotics* **40**, 4252–4264 (2024)
27. Ronneberger, O., Fischer, P., Brox, T.: U-Net: Convolutional Networks for Biomedical Image Segmentation. In: *MICCAI*. pp. 234–241. Springer (2015)
28. Rousseeuw, P.J.: Least Median of Squares Regression. *Journal of the American Statistical Association* **79**(388), 871–880 (1984)
29. Sucar, E., Liu, S., Ortiz, J., Davison, A.J.: iMAP: Implicit Mapping and Positioning in Real-Time. In: *ICCV*. pp. 6229–6238 (2021)
30. Visentini-Scarzanella, M., Sugiura, T., Kaneko, T., Koto, S.: Deep monocular 3D reconstruction for assisted navigation in bronchoscopy. *International Journal of Computer Assisted Radiology and Surgery* **12**(7), 1089–1099 (Jul 2017)
31. Wang, K., Yang, C., Wang, Y., Li, S., Wang, Y., Dou, Q., Yang, X., Shen, W.: EndoGSLAM: Real-Time Dense Reconstruction and Tracking in Endoscopic Surgeries using Gaussian Splatting. *arXiv preprint arXiv:2403.15124* (2024)
32. Wang, R., Pizer, S.M., Frahm, J.M.: Recurrent neural network for (un-) supervised learning of monocular video visual odometry and depth. In: *CVPR*. pp. 5555–5564 (2019)
33. Wang, S., Paruchuri, A., Zhang, Z., McGill, S., Sengupta, R.: Structure-preserving Image Translation for Depth Estimation in Colonoscopy Video. In: *MICCAI*. vol. LNCS 15011, pp. 667–677. Springer (October 2024)
34. Wang, Y., Long, Y., Fan, S.H., Dou, Q.: Neural Rendering for Stereo 3D Reconstruction of Deformable Tissues in Robotic Surgery. In: *MICCAI*. pp. 431–441. Springer (2022)
35. Zhou, Q.Y., Park, J., Koltun, V.: Open3D: A modern library for 3D data processing. *arXiv:1801.09847* (2018)